Proceedings of CONF-FMCE 2025 Symposium: Semantic Communication for Media Compression and Transmission
DOI: 10.54254/2755-2721/2025.GL25346

Research on the Coordinated Optimization Scheduling Strategy of the Multi-Source Power Generation System Incorporating EH-CSP Power Station

Tianqing Gu

School of Electrical Engineering and Automation, Hefei University of Technology, Hefei, China
2022210688@mail.hfut.edu.cn

Abstract. To achieve efficient accommodation of renewable energy and ensure the safe and stable operation of the power system, this paper proposes a day-ahead and intra-day optimal dispatch method for a multi-source power generation system incorporating an Electric Heaters-Concentrating Solar Power (EH-CSP) plant. The proposed model consists of two components: a day-ahead dispatch plan with a 1-hour time resolution, which determines the generation schedule one day in advance based on load demand curves and renewable energy output prediction curves, serving as input variables for the intra-day dispatch; and an intra-day dispatch plan with a 15-minute time resolution over a 4-hour execution cycle. Without considering thermal unit start-up/shutdown costs, the intra-day dispatch first performs rolling optimization for hours 1-4 using day-ahead scheduling data and ultra-short-term load/renewable energy forecasts. Subsequently, it predicts the next hour's load demand and renewable output based on optimized results from hours 1-4, then performs rolling optimization for hours 2-5. This process repeats 24 times to obtain 96-time-point data for load, wind, PV, and EH-CSP plant outputs. Finally, these data are used to determine power source dispatch schedules and system spinning reserve plans. The model is solved using the Curve-Incremental Strategy-based Adaptive Particle Swarm Optimization (CIPSO) algorithm. Case studies on a modified IEEE 30-node system demonstrate that the proposed method effectively enhances renewable energy utilization and reduces operational costs in power systems.

Keywords: EH-CSP Plant, Multi-source Power Generation System, CIPSO Algorithm, Renewable Energy Utilization

1. Introduction

Under the trend of increasingly severe energy shortages and environmental pollution, renewable energy sources such as wind and solar power have experienced rapid development and expanding grid integration due to their abundant reserves and zero-emission, renewable advantages [1]. However, the inherent high volatility and intermittency of renewable energy exacerbate the peak-valley difference in the power system's equivalent load when integrated at scale. This compresses the spinning reserve capacity of conventional power sources, reduces the accommodation space for

DOI: 10.54254/2755-2721/2025.GL25346

renewable energy itself [2], and increases operational challenges, intensifying wind and solar curtailment. Consequently, there is an urgent need to deeply explore additional reserve resources within the grid without increasing carbon emissions [3,4]. Concentrating Solar Power (CSP), particularly thermal storage-equipped CSP plants, represents a promising solar technology with time-shifting and continuously adjustable capabilities, enabling it to provide spinning reserve for the system [5-6]. However, CSP operation is constrained by solar resource availability and thermal storage capacity. Thus, coordinating the allocation of spinning reserve capacities between CSP units and conventional units to maximize renewable energy utilization while ensuring power system stability and security has become a critical research priority.

Existing studies have investigated the coordinated dispatch of CSP plants with thermal power units, wind farms, and photovoltaic plants. Reference [7] established a joint dispatch system for CSP and thermal power units, demonstrating that rational utilization of CSP output significantly reduces system economic costs. Reference [8] developed an optimized operation model for wind-PV-CSP hybrid systems to address power imbalance during peak and off-peak periods, ensuring grid-connected power aligns with dispatch curves. These studies confirm the feasibility of CSP as a flexible power source for providing spinning reserves, offering theoretical foundations for further research. However, they lack effective solutions for constraints imposed by solar irradiation and thermal storage capacity on CSP dispatchability. Some scholars propose integrating electric heaters (EH) with CSP plants to enhance operational flexibility. Reference [9] combined EH-CSP with price-based demand response (PDR) in a wind- photovoltaic (PV) -CSP hybrid system, achieving cost reduction and improved dispatch capability. Reference [10] introduced incentive-based demand response into a wind-PV-EH-CSP co-generation model, enhancing renewable energy utilization while lowering operational costs. While these studies validate that EH-CSP integration promotes wind power accommodation and strengthens reserve capacity, most focus on economic benefits and inadequately address the efficient utilization challenges under high-penetration, large-scale renewable energy integration.

In summary, this paper focuses on coordinating the power outputs of thermal power, CSP plants, and EH with the dual objectives of reducing system operational costs and enhancing wind and solar energy utilization. The study is conducted under a framework of multi-timescale and multi-objective optimization. First, the fundamental generation principles and output models of EH-CSP plants are introduced. Building on this, a day-ahead and intra-day optimal dispatch model for a multi-source power generation system incorporating EH-CSP plants is proposed. The model is solved using the CIPSO algorithm. Finally, case study simulations verify the effectiveness of the proposed model.

2. Operational mechanism of EH-CSP plant

A CSP plant primarily consists of three components: the solar field (SF), thermal energy storage (TES), and power block (PB) [11]. The heat transfer fluid (HTF) facilitates energy transfer among these components. The solar field absorbs solar energy and uses thermal conversion equipment to heat the HTF, converting solar energy into thermal energy. A portion of this thermal energy is converted into electricity via steam turbine units, while the remainder is stored in the TES. The TES releases stored thermal energy to the power block via the HTF when needed [12]. An EH, which converts electrical energy into thermal energy, is typically implemented in three practical forms: electrode-based, electromagnetic induction-based, and resistive heaters [13]. This study employs a resistive molten salt electric heater as the EH device.

The system integrating EH and CSP plants is illustrated in Figure 1. Compared to conventional CSP plants, the heat-conducting molten salt in the thermal storage system absorbs not only thermal

DOI: 10.54254/2755-2721/2025.GL25346

energy from the solar field's photothermal conversion but also additional heat generated by the EH through electric heating during its flow from the low-temperature to high-temperature molten salt tanks. This integration reduces the dependency on solar irradiation for CSP generation capacity. Furthermore, the EH, functioning as an adjustable load, can provide reserve capacity for the system by modulating its power consumption.

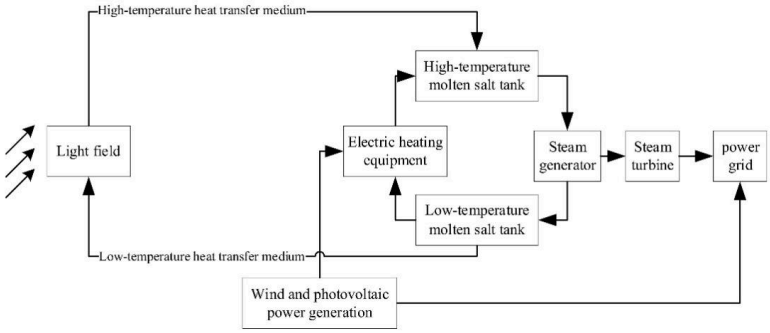

Figure 1. EH-CSP plant structural system diagram

The thermal power absorbed by the CSP plant is expressed as:

$$P_t^{th,solar} = \eta_{SF} S_{SF} D_t \tag{1}$$

Where: η_{SF} is the solar-to-thermal conversion efficiency of the solar field (unit: %); S_{SF} is the total area of the solar field (unit: hm^2); D_t is the direct normal irradiance (DNI) at time t (unit: w/m^2); $P_t^{th,solar}$ represents the thermal power absorbed by the solar collector during time period t (unit: MW).

The thermal energy absorbed by the solar collector is utilized to generate electricity during peak load periods, while during off-peak periods, it is transferred to the TES (Thermal Energy Storage) for storage. The stored thermal energy is then released during subsequent peak load periods to produce electricity.

$$P_t^{th,solar} = P_t^{th,H-P} + P_t^{th,H-T} \tag{2}$$

Where: $P_t^{th,H-P}$: thermal power **directly utilized for electricity generation by the solar collector at time t (unit: MW); $P_t^{th,H-T}$: thermal power supplied to the TES by the solar collector at time t (unit: MW).

Thermal losses occur during both charging and discharging processes, and charging and discharging cannot be conducted simultaneously. The charge-discharge characteristics are thus defined as:

$$\begin{cases} P_t^c = \eta_c P_t^{th,H-T} \\ P_t^d = \frac{P_t^{T-H}}{\eta_d} \\ P_t^c P_t^d = 0 \end{cases} \tag{3}$$

Where: P_t^c and P_t^d : charging and discharging thermal power at time t (unit: MW); η_c and η_d : charging and discharging efficiencies (unit: %); P_t^{T-H} : thermal energy transferred from TES to

DOI: 10.54254/2755-2721/2025.GL25346

HTF at time t (unit: MW).

The thermal energy stored in the TES, accounting for energy dissipation, is expressed as:

$$E_t = e^{-\delta \Delta t} E_{t-1} + \left(P_{t-1}^c - P_{t-1}^d\right) \Delta t \tag{4}$$

Where: E_t : thermal energy stored in the TES at time t ; ; : dissipation coefficient; Δt : time interval.

The electrical power output of the CSP plant is derived from thermal energy supplied by both the solar collector and thermal storage system, expressed as:

$$P_{csp\_t} = \eta_f \left(P_t^{th,solar} - \frac{P_t^c}{\eta_c} + P_t^d \eta_d + E_{t,EH}\right) \tag{5}$$

Where: η_f : thermal-to-electric conversion efficiency of the CSP plant (unit: %); $E_{t,EH}$: thermal power generated by the EH at time t (unit: MW); P_{csp_t} : electrical power output of the CSP plant at time t (unit: MW).

The EH, as a critical electro-thermal conversion component in the CSP plant, achieves a conversion efficiency of nearly 100% [14]. Its thermal output is determined by the curtailed wind and solar power, modeled as:

$$E_{t,EH} = \eta_{EH} P_t^{EH} \tag{6}$$

Where: P_t^{EH} : input electrical power to the EH at time t ; η_{EH} : electro-thermal conversion efficiency of the EH under steady-state operation.

The thermal output is constrained by:

$$0 <; E_{t,EH} <; E_{EH}^{max} \tag{7}$$

Where: E_{EH}^{max} denotes the maximum thermal power output limit of the EH.

3. Optimization of wireless charging system

This study proposes a day-ahead and intra-day optimal dispatch model for a multi-source power generation system incorporating EH-CSP plants, targeting maximization of daily renewable energy generation and minimization of system operational costs. The model comprises two components: a day-ahead dispatch plan and an intra-day dispatch plan, as illustrated in Figure 2.

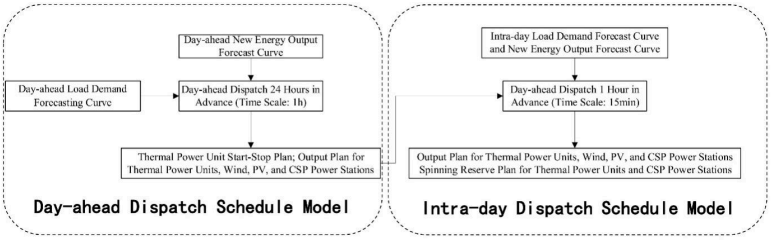

Figure 2. Dispatch model structure diagram

The day-ahead dispatch plan operates with a time scale of 1 hour, formulated one day in advance. Based on the predicted load demand curve and renewable energy output forecast curves, it

DOI: 10.54254/2755-2721/2025.GL25346

determines the start-up and shutdown schedules for thermal power units and the dispatch output plans for thermal power, wind power, PV and CSP plants. The day-ahead dispatch results serve as input variables for the intra-day dispatch plan.

The intra-day dispatch plan operates with a time scale of 15 minutes and an execution cycle of 4 hours. Without considering the start-up and shutdown costs of thermal power units, it prioritizes rolling optimization for the first 1-4 hours based on day-ahead dispatch data and ultra-short-term load demand and renewable energy output forecasts. Using the optimized load, PV, wind, and CSP data, the system predicts the next hour's load demand and renewable energy output, then rolling optimizes 2-5 hours. This process repeats 24 times to obtain dispatch output data for 96 time points across wind, PV, CSP, and thermal power units. Finally, by adjusting the output of all power sources, the dispatch output plans for each power source and the system spinning reserve plan are determined.

3.1. Day-ahead dispatch plan model

3.1.1. Day-ahead dispatch plan model objective function

(1) Maximization of Daily Power Output for CSP, PV, and Wind Power

$$f_1 = \max \sum_{t=1}^{T} \left(p_{csp\_t} + p_{v\_t} + p_{wind\_t}\right) \tag{8}$$

Where: p_{csp_t}, p_{v_t} and p_{wind_t} represent the dispatch outputs of the CSP, PV, and wind power at time t, respectively; T is the dispatch duration of the scheduling day, with $T ; = 24$ hours.

(2) Minimization of Comprehensive Operational Cost

$$\min f_2 = (C_{11} + C_2 + C_3 + C_4) \tag{9}$$

Where: f_2 : total operational cost; C_{11} : generation cost of thermal power units in the day-ahead dispatch plan; C_2 : operation and maintenance(O&;M) costs for wind, PV, and CSP generation; C_3 : penalty costs for wind and solar curtailment; C_4 : system spinning reserve capacity cost.

The generation cost of thermal power units in the day-ahead dispatch plan, C_{11}, is expressed as:

$$C_{11} = p_{it} \sum_{t=1}^{T} \sum_{i=1}^{n} \left[a_i p_{it}^2 + b_i p_{it} + c_i\right] + u_{it} \sum_{t=1}^{T} \sum_{i=1}^{n} \left[u_{it}\left(1 - u_{i(t-1)}\right) S_i\right] \tag{10}$$

Where: p_{it} : electrical power output of thermal unit i at time t (unit: MW); u_{it} : operational status of thermal unit i at time t ($u_{it} = 1$ for online, $u_{it} = 0$ for offline); a_i, b_i, c_i : fuel cost coefficients of thermal unit i ; n : total number of thermal units.

The operation and maintenance cost for wind, PV, and CSP generation, C_2, is expressed as:

$$C_2 = k_j \eta_d p_t^{SF,r} + k_{Ts}\left(1 - \eta_f\right) \eta_d p_t^{TS,f} + k_w p_{wind\_t} + k_v p_{v\_t} \tag{11}$$

Where: $p_t^{SF,r}$: thermal power directly used for generation by the solar collector at time t ; $p_t^{TS,f}$: thermal power supplied by TES discharge at time t ; η_d : thermal-to-electric conversion efficiency; η_f : heat loss rate of the TES; k_j, k_{Ts} : O&;M cost coefficients for solar field-based and TES-based CSP generation; k_w, k_v : O&;M cost coefficients for wind and PV generation; p_{wind_t}, p_{v_t} : power outputs of wind and PV at time t .

DOI: 10.54254/2755-2721/2025.GL25346

The penalty cost for wind and solar curtailment, C_3, is expressed as:

$$C_3 = k_{wc} p^{c}_{wind\_t} + k_{vc} p^{c}_{v\_t} \tag{12}$$

Where: k_{wc}, k_{vc}: penalty coefficients for wind and solar curtailment; $p^{c}_{wind\_t}$, $p^{c}_{v\_t}$: curtailed wind and solar power at time t.

The system spinning reserve capacity cost, C_4, is expressed as:

$$C_4 = k_i \left(U_{it} + D_{it}\right) + k_c \left(p^{Up}_{csp\_t} + p^{Down}_{csp\_t}\right) + k_e \left(p^{Up}_{eh\_t} + p^{Down}_{eh\_t}\right) \tag{13}$$

Where: k_i, k_c, k_e: spinning reserve cost coefficients for thermal units, CSP plants, and EH; U_{it}, D_{it}: upward/downward spinning reserve capacities of thermal unit i at time t; $p^{Up}_{csp\_t}$, $p^{Down}_{csp\_t}$: upward/downward spinning reserves from the CSP plant; $p^{Up}_{eh\_t}$, $p^{Down}_{eh\_t}$: upward/downward spinning reserves from the EH.

3.1.2. Constraints

(1) The power balance constraint for the integrated system

$$\sum_{i=1}^{N} p_{it} + p_{csp\_t} + p_{wind\_t} + p_{v\_t} = p_{f\_t} \tag{14}$$

Where: p_{f_t}: forecasted load demand power at time t.

(2) Thermal Power Unit Operational Constraints

The upward and downward spinning reserve capacity constraints are formulated as:

$$\begin{cases} U_{it} = \sum_{i=1}^{n} \left(p_{i\_max} - p_{it}, r_{ui}\right) \geq p_{c\_t} = p_{f\_t} L \\ D_{it} = \sum_{i=1}^{n} \left(p_{it} - p_{i\_min}, r_{di}\right) \geq p_{c\_t} = p_{f\_t} L \end{cases} \tag{15}$$

Where: p_{i_max}, p_{i_min}: upper and lower output limits of thermal unit i; r_{ui}, r_{di}: maximum upward and downward ramping rates of unit i; p_{c_t}: forecast error of system load.

Power Output Constraints of Thermal Units

$$p_{i\_min} \leq p_{it} \leq p_{i\_max} \tag{16}$$

Ramping Rate Constraints of Thermal Units

$$-r_{di} \leq p_{it} - p_{i(t-1)} \leq r_{ui} \tag{17}$$

Power Output Constraints During Start-Up/Shut-Down

$$p_{it} = p_{i\_min} = \begin{cases} u_{i(t-1)} = 0, u_{it} = 1 \\ u_{it} = 1, u_{i(t+1)} = 0 \end{cases} \tag{18}$$

This equation indicates that when a thermal unit transitions from offline to online or online to offline, its power output during that interval is set to the minimum stable operating output.

(3) Operational Constraints of the CSP Plant

DOI: 10.54254/2755-2721/2025.GL25346

Thermal Storage Capacity Constraints

$$\mathrm{E}_{\min}^{\mathrm{th}} \leq \mathrm{E}_{\mathrm{t}}^{\mathrm{th}} \leq \mathrm{E}_{\max}^{\mathrm{th}} = \mathrm{m}^{\mathrm{TEX}} \mathrm{p}_{\mathrm{csp\_max}} \tag{19}$$

Where: $\mathrm{E}_{\max}^{\mathrm{th}}$, $\mathrm{E}_{\min}^{\mathrm{th}}$: upper and lower limits of TES thermal storage capacity; $\mathrm{m}^{\mathrm{TEX}}$: maximum TES capacity in full-load hours (FLH); $\mathrm{p}_{\mathrm{csp\_max}}$: maximum power output of the CSP plant.

Thermal Charge/Discharge Power Constraints

$$\begin{cases} 0 \leq \mathrm{p}_{\mathrm{t}}^{\mathrm{th,c}} \leq \mathrm{p}_{\max}^{\mathrm{th,c}} \\ 0 \leq \mathrm{p}_{\mathrm{t}}^{\mathrm{th,d}} \leq \mathrm{p}_{\max}^{\mathrm{th,d}} \end{cases} \tag{20}$$

Where: $\mathrm{p}_{\max}^{\mathrm{th,c}}$, $\mathrm{p}_{\max}^{\mathrm{th,d}}$ are the maximum thermal charge and discharge power rates.

Mutual Exclusion of Charge/Discharge in the Same Interval

$$\mathrm{p}_{\mathrm{t}}^{\mathrm{th,c}} \mathrm{p}_{\mathrm{t}}^{\mathrm{th,d}} = 0 \tag{21}$$

Power Output Constraints

$$\mathrm{p}_{\mathrm{csp\_min}} \leq \mathrm{p}_{\mathrm{csp\_t}} \leq \mathrm{p}_{\mathrm{csp\_max}} \tag{22}$$

Where: $\mathrm{p}_{\mathrm{csp\_min}}$ is the minimum power output of the CSP plant.

Ramping Rate Constraints

$$-\mathrm{r}_{\mathrm{d\_csp}} \leq \mathrm{p}_{\mathrm{csp\_t}} - \mathrm{p}_{\mathrm{csp\_(t-1)}} \leq \mathrm{r}_{\mathrm{u\_csp}} \tag{23}$$

Where: $\mathrm{r}_{\mathrm{u\_csp}}$, $-\mathrm{r}_{\mathrm{d\_csp}}$ are the maximum upward and downward ramping rates.

Spinning Reserve Capacity Constraints

$$\begin{cases} \mathrm{p}_{\mathrm{csp\_t}}^{\mathrm{Up}} \leq \mathrm{p}_{\mathrm{csp\_max}} - \mathrm{p}_{\mathrm{csp\_t}} \\ \mathrm{p}_{\mathrm{csp\_t}}^{\mathrm{Down}} \leq \mathrm{p}_{\mathrm{csp\_t}} - \mathrm{p}_{\mathrm{csp\_min}} \end{cases} \tag{24}$$

(4) EH Operational Constraints

Power Output Constraints

$$0 \leq p_{eh_t} = k_{we}(P_{W_t} - P_{wind_t} - P_{wind_t}^{c}) + k_{ve}(P_{V_t} - P_{v_t} - P_{v_t}^{c}) \leq p_{EH} \tag{25}$$

Where: $\mathrm{p}_{\mathrm{eh\_t}}$: power output of the EH at time t ; p_{EH} : rated power capacity of the EH; $\mathrm{P}_{\mathrm{W\_t}}$, $\mathrm{P}_{\mathrm{V\_t}}$: forecasted wind and PV power outputs at time t ; k_{we} , k_{ve} : absorption coefficients of the EH for surplus wind and PV power.

(5) Spinning Reserve Capacity Constraints

$$\begin{cases} \mathrm{p}_{\mathrm{eh\_t}}^{\mathrm{Up}} \leq \mathrm{p}_{\mathrm{EH}} - \mathrm{p}_{\mathrm{eh\_t}} \\ \mathrm{p}_{\mathrm{eh\_t}}^{\mathrm{Down}} \leq \mathrm{p}_{\mathrm{eh\_t}} \end{cases} \tag{26}$$

DOI: 10.54254/2755-2721/2025.GL25346

Wind Farm Power Output Constraints

$$0 \le P_{wind\_t} \le P_{wind\_max} \tag{27}$$

(6) PV Power Plant Output Constraints

$$0 \le P_{v\_t} \le P_{v\_max} \tag{28}$$

3.2. Intra-day dispatch plan model

3.2.1. Objective function

(1) Maximization of Daily Power Output for CSP, PV, and Wind Power

$$f_3 = \max \sum_{t=1}^{T} (p_{wind\_t} + p_{v\_t} + p_{csp\_t}) \tag{29}$$

(2) Minimization of Comprehensive Operational Cost

$$\min f_4 = (C_{12} + C_2 + C_3 + C_4) \tag{30}$$

The generation cost of thermal power units in the intra-day dispatch plan, C_{12}, is expressed as:

$$C_{12} = p_{it} \sum_{t=1}^{T} \sum_{i=1}^{n} \left[a_i p_{it}^2 + b_i p_{it} + c_i\right] \tag{31}$$

3.2.2. Constraints

The intra-day dispatch plan model shares the same specific constraints as the day-ahead dispatch plan model and will not be reiterated here.

3.3. Model solution

3.3.1. Day-ahead dispatch plan model

The model proposed in this study is a multi-objective optimization problem. By assigning different weighting coefficients to each objective function, the multi-objective problem can be transformed into a single-objective problem for solution. In the day-ahead dispatch plan model, which includes two objective functions f_1 and f_2, their coordination is addressed as:

$$A = \min\left(\lambda_1 \frac{f_{1max} - f_1}{f_{1max} - f_{1min}} + \lambda_2 \frac{f_2 - f_{2min}}{f_{2max} - f_{2min}}\right) \tag{32}$$

Where: λ_1, λ_2 : linear weighting coefficients for f_1 and f_2, respectively, with $\lambda_1 + \lambda_2 = 1$ and λ_1, $\lambda_2 \in [0,1]$; f_{1max}, f_{2max} : optimal solutions (best values) for f_1 and f_2; f_{1min}, f_{2min} : worst solutions (poorest values) for f_1 and f_2.

The intra-day dispatch plan model follows a similar approach:

$$B = \min\left(\lambda_3 \frac{f_{3max} - f_3}{f_{3max} - f_{3min}} + \lambda_4 \frac{f_4 - f_{4min}}{f_{4max} - f_{4min}}\right) \tag{33}$$

DOI: 10.54254/2755-2721/2025.GL25346

where: λ_3 , λ_4 : linear weighting coefficients for f_3 and f_4 , respectively, with $\lambda_3 + \lambda_4 = 1$ and λ_3 , $\lambda_4 \in [0,1]$; f_{3max} , f_{4max} : optimal solutions (best values) for f_3 and f_4 ; f_{3min} , f_{4min} : worst solutions (poorest values) for f_3 and f_4 .

The focus of this study is to address the green and efficient absorption of renewable energy after large-scale grid integration. Therefore, we prioritize f_1 over f_2 and f_3 over f_4 . Accordingly, the weighting coefficients are set as: λ_1 slightly larger than λ_2 ; λ_3 slightly larger than λ_4 .

3.3.2. CIPSO algorithm

To address the limitations of the traditional Particle Swarm Optimization (PSO) algorithm, such as its sensitivity to the initial population's positional states, poor global search capability, significant reduction in population diversity, and premature convergence in later stages[15], this study employs the CIPSO algorithm for model solving. The workflow of the CIPSO algorithm for solving the model is illustrated in Figure 3.

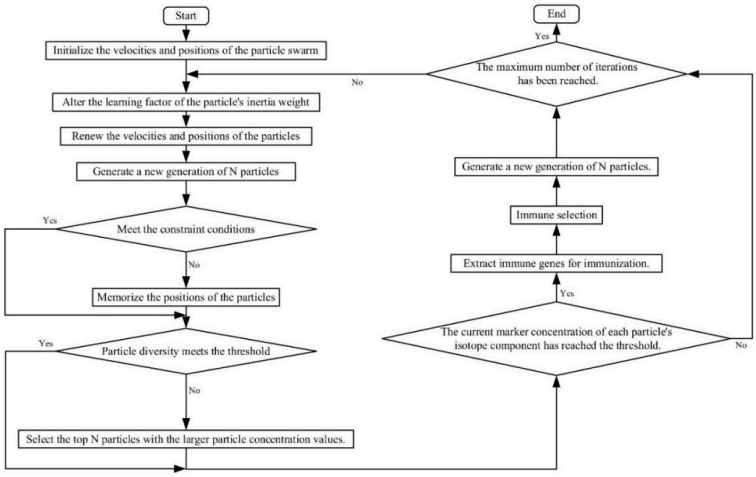

Figure 3. Algorithm flowchart

4. Case study analysis

4.1. Case study overview

This paper adopts a modified IEEE 30-node system to validate the effectiveness of the proposed day-ahead and intra-day optimal scheduling method for a multi-source power generation system incorporating EH-CSP plants. The CSP plant equipped with EH devices are connected to Node 1, the Wind Turbine Generator Systems (WTGS) is connected to Node 2, the PV power plant is connected to Node 5, and thermal power units are connected to Nodes 8, 11, and 13. The modified network topology is shown in Figure 4.

DOI: 10.54254/2755-2721/2025.GL25346

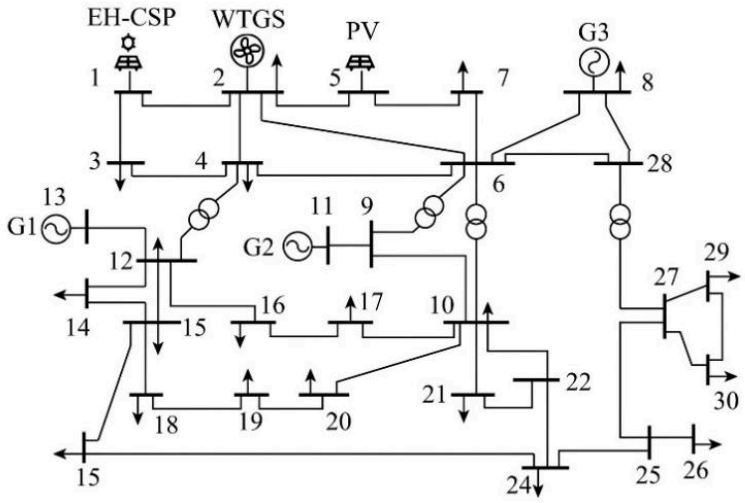

Figure 4. Modified IEEE 30-node system

The installed capacities of the wind farm and PV power plant participating in system dispatch are 480 MW and 150 MW, respectively. The rated capacity of the EH is $P_{EH} = 50MW$ and the system load forecast error rate is $L ; = 0.05$. The operation and maintenance cost coefficients for wind and PV power are $k_w = 20yuan/MW$ and $k_v = 30yuan/MW$ respectively. The CSP plant's operation and maintenance cost coefficients are $k_i = 20yuan/MW$ (for solar collector-based power generation) and $k_{Ts} = 40yuan/MW$ (for thermal storage-based power generation). The penalty cost coefficients for wind and PV curtailment are $k_{wc} = 100$ and $k_{vc} = 100$ respectively. The spinning reserve cost coefficients for thermal units, the CSP plant, and the EH are $130yuan/MW$, $50yuan/MW$ and $40yuan/MW$ respectively.

The detailed operational parameters of the CSP plant are listed in Table 1, and the parameters of the three thermal units are provided in Table 2.

DOI: 10.54254/2755-2721/2025.GL25346

Table 1. CSP plant regulation parameters

Parameter	Value
Rated output power of CSP plant / MW	150
Minimum output power during CSP operation / MW	10
Maximum ramping rate of CSP plant / MW/h	40
CSP thermoelectric conversion efficiency / %	45
CSP photothermal conversion efficiency / %	57
Mirror field area / m²	1.34×10^6
Discharge loss rate of TES / %	3
Daily maximum thermal storage capacity of TES / MW·h	1000
Initial thermal storage capacity of TES / MW·h	400
Lower limit of TES thermal storage / MW·h	100
Thermal dissipation coefficient of TES / %	3.1
Thermal charging efficiency of TES / %	98.58
Thermal discharging efficiency of TES / %	98.56
Cost coefficient for collector-based power generation / yuan/MW·h	20
Cost coefficient for thermal storage-based power generation / yuan/MW·h	40

Table 2. Parameters of thermal units

Unit	Upper Output Limit (MW)	Lower Output Limit (MW)	Ramping Rate (MW/h)	Fuel Cost Coefficients			Start-Up/Shut-Down Cost Coefficient (yuan/MW)
				a_i	b_i	c_i	h_i
				yuan / MW^2	yuan / MW	yuan	yuan / MW
G1	80	40	40	0.0031	175	350	1729
G2	50	18	18	0.0023	100	1250	1982
G3	35	12	12	0.0015	225	167	2464

4.2. Case study results

To validate the effectiveness of the proposed dispatch method, three operational modes are defined:

Mode 1: No participation of CSP plants or EH. Optimal dispatch is performed only for the system composed of wind, PV, and thermal units.

Mode 2: Building upon Mode 1, CSP plants are incorporated into the system dispatch.

Mode 3: Further expanding on Mode 2, EH participation is added to the system dispatch.

The simulation of the three modes is conducted under the same typical day.

DOI: 10.54254/2755-2721/2025.GL25346

4.2.1. Unit output results under different modes

Figures 5, 6, and 7 show the power output results of thermal units, CSP plants, wind, and PV under the three operational modes, respectively.

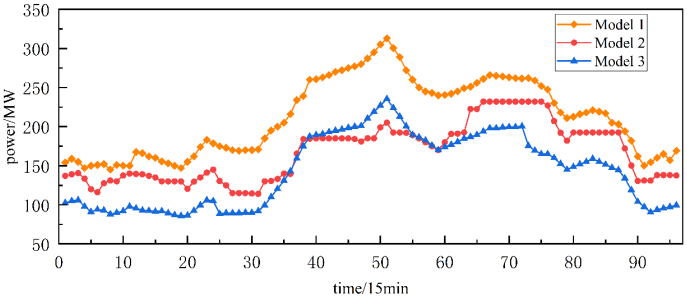

Figure 5. Power output results of thermal units

Although the power output of thermal units in Mode 2 is smoother compared to Mode 3 and Mode 1, its total output is significantly higher than that of Mode 3, resulting in less pronounced advantages in terms of dispatch economy. In Mode 3, the power output of thermal units is only 69.2% of Mode 1 and 82.33% of Mode 2, demonstrating superior economic efficiency.

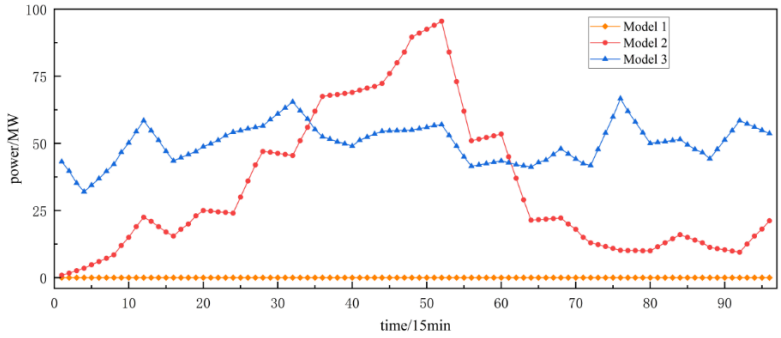

Figure 6. Power output results of CSP plant

In Mode 1, the CSP plant does not participate in dispatch, and its power output is 0. Due to the joint participation of the EH and CSP plant in system dispatch, the power output of the CSP plant in Mode 3 is significantly greater than that in Mode 2, and the output is more stable. The power output of the CSP plant in Mode 2 is only 67.66% of that in Mode 3.

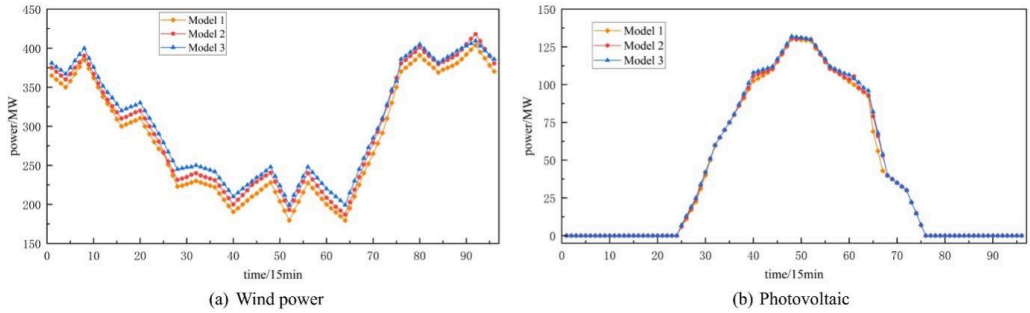

Figure 7. Wind and PV power output results

DOI: 10.54254/2755-2721/2025.GL25346

In the three dispatch modes, the grid-connected power of wind and PV increases sequentially. The wind power output in Mode 1 is 94.24% of that in Mode 3, and the PV power output is 98.62% of that in Mode 3. The wind power output in Mode 2 is 97.61% of that in Mode 3, and the PV power output is 98.10% of that in Mode 3.

4.2.2. System spinning reserve allocation results under different modes

Figures 8, 9, and 10 show the allocation plans for the upward spinning reserve capacity required by the system under the three modes, respectively.

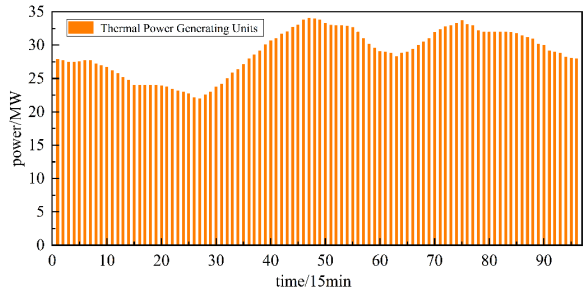

Figure 8. Spinning reserve capacity in mode 1

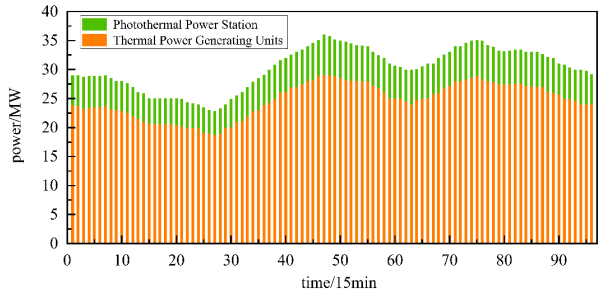

Figure 9. Spinning reserve capacity in mode 2

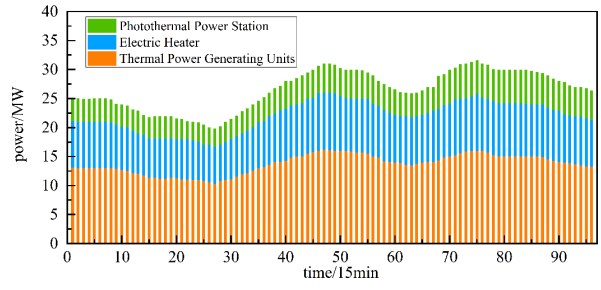

Figure 10. Spinning reserve capacity in mode 3

In Mode 1, the system's spinning reserve capacity is entirely provided by thermal units. In Mode 2, the CSP plant and thermal units jointly provide the spinning reserve capacity. In Mode 3, the EH is further added to participate. Therefore, in the optimized dispatch of Mode 3, compared to Modes 1 and 2, the reserve pressure on thermal units is significantly reduced, and the upward spinning reserve capacity decreases by 365.83 MW and 263.97 MW, respectively.

DOI: 10.54254/2755-2721/2025.GL25346

4.2.3. System wind and PV power absorption under different modes

Figure 11 shows the curtailed wind power and curtailed PV power of the system under the three modes.

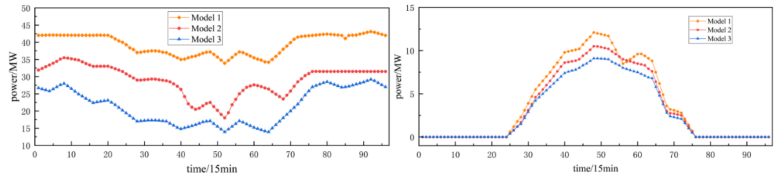

Figure 11. Spinning reserve capacity in mode 3

Table 3 shows the actual wind and PV power absorption under the three modes.

Table 3. Comparison of wind and PV power absorption under different modes

Parameter	Day-Ahead			Intra-Day		
	Mode 1	Mode 2	Mode 3	Mode 1	Mode 2	Mode 3
Wind Power Absorption/%	86.87	90.96	92.66	88.09	91.05	93.16
PV Power Absorption/%	89.72	91.54	92.18	90.33	92.98	93.75

In Mode 1, since CSP plants and EH are not considered, the forecast errors of wind and PV power outputs are compensated solely by adjusting the output of thermal units. Although Mode 2 incorporates CSP plants and thermal units to jointly compensate for wind and PV forecast errors, the actual absorption of wind power does not reach the expected level. In Mode 3, by coordinately regulating thermal units, CSP plants, and EH to compensate for wind and PV forecast errors, the absorption rates of wind and PV power are significantly increased.

4.2.4. Total dispatch cost under different modes

Table 4. Comparison of actual total dispatch costs under different modes

Parameter	Day-Ahead			Intra-Day		
	Mode 1	Mode 2	Mode 3	Mode 1	Mode 2	Mode 3
Total Cost (10^4 yuan)	117.65	114.77	109.97	114.55	112.87	103.43

As shown in Table 3.3, Mode 3 achieves the lowest total dispatch cost. In the day-ahead dispatch, Mode 3 reduces the dispatch cost by 6.53% and 4.18% compared to Modes 1 and 2, respectively. In the intra-day dispatch, the cost reductions are 9.71% and 8.36% compared to Modes 1 and 2, respectively. Under the same mode, the intra-day dispatch cost of Mode 3 is 65,400 yuan lower than its day-ahead dispatch cost, demonstrating significant improvement in the system's operational economy under Mode 3.

5. Conclusion

To address the intensified peak-valley difference in the equivalent load of power systems and the "wind/PV curtailment" phenomena caused by large-scale integration of renewable energy, this paper

DOI: 10.54254/2755-2721/2025.GL25346

proposes a day-ahead and intra-day optimal dispatch method for a multi-source generation system incorporating EH-CSP plants. By leveraging the dispatchability of EH-CSP plants and the complementary characteristics of renewable energy outputs, the proposed method establishes a coordinated multi-timescale and multi-objective optimization strategy. This approach effectively enhances wind and PV power absorption while reducing system operational costs. The research findings provide valuable insights for the rational dispatch of power systems with high-penetration renewable energy integration.

Due to time constraints, this paper focuses only on the coordinated optimal scheduling across the day-ahead and intraday time scales. Additionally, the study emphasizes theoretical modeling, with limited exploration of solution algorithms. Future research could extend to multi-time-scale optimization (e.g., week-ahead, day-ahead, intraday, and real-time scheduling) and analyze the performance of various solution algorithms to identify more efficient solving approaches.

References

[1] Cui Yang, Yang Zhiwen, Zhang Jietan, et al. Joint Output Scheduling Strategy of Wind Power, Photovoltaic Power and Solar Thermal Power Considering Comprehensive Cost [J]. High Voltage Technology, 2019, 45(01): 269-275.
[2] Zhang Yaoxiang, Liu Wenying, Pang Qinglun, et al. Optimization Method of Rotating Reserve for Thermal Power and Solar Thermal Power in High Proportion Wind Power Grids [J]. Transactions of China Electrotechnical Society, 2022, 37(21): 5478-5489.
[3] Carry Forward the Past and Open Up the Future: Embark on a New Journey of Global Response to Climate Change: Speech at the Climate Ambition Summit [N]. People's Daily, 2020-12-13(2).
[4] Chen Guoping, Dong Yu, Liang Zhifeng. Analysis and Reflection on the High-Quality Development of New Energy with Chinese Characteristics in Energy Transition [J]. Proceedings of the CSEE, 2020, 40(17): 5493-5505.
[5] Lin Keming, Wang Zhaoheng, Wu Feng, et al. Dynamic Modeling and Power Coordination Control of Photovoltaic-Thermal Combined Power Generation System [J]. Electric Power Automation Equipment, 2021, 41(9): 110-117.
[6] Zhu Rui, Hu Bo, Xie Kaigui, et al. Time-Sequential Stochastic Production Simulation of Multi-Energy Power System Containing Wind Power, Photovoltaic, Solar Thermal, Hydropower, Thermal Power and Energy Storage [J]. Power System Technology, 2020, 44(9): 3246-3253.
[7] Cui Yang, Yang Zhiwen, Zhong Wuzhi, et al. Day-Ahead Dispatch of Thermal Storage Solar Thermal Power Station and Thermal Power Unit Based on Cost Optimization [J]. Electric Power Automation Equipment, 2019, 39(02): 71-77.
[8] Sun Ke, Zhao Shuqiang, Li Zhiwei. Research on Joint Optimization Operation of Wind-PV-Solar Thermal Power Generation System [J]. Journal of North China Electric Power University (Natural Science Edition), 2024, 51(2): 70-79, 89. DOI: 10.3969/j.ISSN.1007-2691.2024.02.08.
[9] Cui Yang, Zhang Jiarui, Wang Zheng, et al. Day-Ahead Dispatch Strategy of Wind-PV-Solar Thermal Combined Power Generation System Considering Price-Type Demand Response [J]. Proceedings of the CSEE, 2020, 40(10): 3103-3114.
[10] Yang Beijia, Zhao Qingsong, Liu Gang, et al. Optimal Dispatch of Wind-PV-Thermal Combined Power Generation Considering Demand Response [J]. Northeast Electric Power Technology, 2024, 45(3): 1-6, 12. DOI: 10.3969/j.issn.1004-7913.2024.03.001.
[11] Zhang Jinping, Zhou Qiang, Wang Dingmei, et al. Review of Solar Thermal Power Generation Technology and Its Development [J]. Integrated Energy, 2023, 45(2): 44-52.
[12] Xiong Wei, Ma Zhicheng, Zhang Xiaoying, et al. Two-Layer Optimization Dispatch of Wind-PV-Solar Thermal Complementary Power Generation Considering Wind and Solar Energy Absorption [J]. Acta Energiae Solaris Sinica, 2022, 43(7): 39-48.
[13] Liu Yi. Research on Optimal Dispatch of Multi-Source Power Generation System with Electric Heating Devices and Solar Thermal Power Stations [D]. East China Jiaotong University, 2021.
[14] Dong Haiying, Yun Yunyun, Ma Zhicheng, et al. Low-Carbon Optimization Operation of Integrated Energy System Considering Multi-Energy Conversion and Participation of Solar Thermal Power Stations [J]. Power System Technology, 2020, 44(10): 3689-3700.

DOI: 10.54254/2755-2721/2025.GL25346

[15] Ge Yingjian. Research on Phase Difference Coherent Detection Technology Based on Improved Particle Swarm Optimization Algorithm [D]. University of Chinese Academy of Sciences (Institute of Optics and Electronics, Chinese Academy of Sciences), 2021.